High-Chroma, High-Contrast Tunable Color Coatings Using Sb2S3 in a Metal-Dielectric Stack

Riley Shurvinton, Arjun Karimbana, Priya Dominic, Antonin Moreau, Olivier Hector, Konstantinos Iliopoulos, Fabien Lemarchand, Julien Lumeau

ADVANCED PHOTONICS RESEARCH
Open Access
www.adpr-journal.com

High-Chroma, High-Contrast Tunable Color Coatings Using Sb_2S_3 in a Metal-Dielectric Stack

Riley Shurvinton, Arjun Karimbana, Priya Dominic, Antonin Moreau, Olivier Hector, Konstantinos Iliopoulos, Fabien Lemarchand, and Julien Lumeau**

Thin-film coatings are a versatile option for creating color. These coatings can be made tunable by introducing phase-change materials (PCMs), whose optical response changes due to an external signal. However, commonly used PCMs such as $Ge_2Sb_2Te_5$ (GST) are limited in their applications for color coatings, due to high absorption of visible light. Here, the alternative PCM Sb_2S_3 is used, and a novel coating design is demonstrated, which incorporates the PCM layer into an asymmetric Fabry–Perot cavity with Ag, SiO_2 and Ti layers. Simulations are used to show that this design yields high-chroma colors in a wide range of hues, which exhibit a large tunable hue shift when the phase of the Sb_2S_3 layer changes. Three coatings are deposited to experimentally verify these results, which give good agreement with the simulations. The phase change of the Sb_2S_3 layer is demonstrated using direct heating using a hotplate, and also using laser annealing, which allows microscale image writing to be realized on the coatings.

1. Introduction

Thin-film stacks are a powerful and well-controlled option for generating color. By using thin layers of materials (typically tens to hundreds of nanometers thick), interference effects occur to create a reflectance (or transmittance) spectrum that depends on the thickness and refractive index of each layer. For example, a three-layer stack using alternating layers of metal-dielectric-metal behaves analogously to an asymmetric Fabry–Perot cavity in reflectance, where the resonance conditions depend on the thickness of the dielectric layer. With proper material choice, this stack can be used to create highly saturated color in a wide variety of hues, making it a versatile option for precise color control.[1]

R. Shurvinton, A. Karimbana, P. Dominic, A. Moreau, O. Hector, K. Iliopoulos, F. Lemarchand, J. Lumeau
Aix Marseille Univ
CNRS, Centrale Med
Institut Fresnel
13013 Marseille, France
E-mail: riley.shurvinton@gmail.com; julien.lumeau@fresnel.fr

The ORCID identification number(s) for the author(s) of this article can be found under https://doi.org/10.1002/adpr.202400194.

DOI: 10.1002/adpr.202400194

Another advantage of thin-film coatings is that they may be made active and tunable by the inclusion of a phase-change material (PCM). PCMs are a class of materials, which have two or more solid phases, with a large optical contrast between them. An external signal, such as a laser or heater, causes the PCM to switch between its phases, which changes the refractive index of the PCM. When incorporated into a thin-film stack, this phase change can be exploited to yield tunable color, where the color of the coating depends on the phase of the PCM layer.

Many PCMs have been studied for active photonics using thin-film coatings. However, the most widely used PCMs, such as $Ge_2Sb_2Te_5$ (GST), have limited use for visible photonics, due to a high absorbance for visible wavelengths of light (380–780 nm). An alternative PCM, antimony trisulfide (Sb_2S_3), has seen significant interest for visible photonics in recent years, due to its lower absorption and large optical contrast.[2,3] However, previous demonstrations of color coatings using Sb_2S_3[2,4–7] have been limited by complex many-layered designs, a restricted gamut (range of colors that can be obtained), a low chroma (saturation or "strength" of color), or a low optical contrast between the amorphous and crystalline phases of the coating.

In this work, we seek to demonstrate a coating design with a low number of layers that can fulfill three key goals: a wide gamut of possible colors, covering as much of the visible color space as possible; a high chroma and brightness; and a large optical contrast between amorphous and crystalline phases. In particular, we seek to show a large difference in hue between phases, enabling the coating to exhibit as large a range of intermediate colors as possible.

To fulfill these goals, we propose a coating design based on a Fabry–Perot cavity with a layer of Sb_2S_3 between the opaque lower mirror and the cavity material. This design allows a wide gamut of colors to be generated by tuning the thickness of the cavity layer, but also maximizes the optical contrast between the amorphous and crystalline phases of Sb_2S_3. We use simulations to find the coating designs with the optimal hue shift. Selected coatings are fabricated using electron beam evaporation, and show good agreement with the simulated predictions. We also demonstrate switching between the amorphous and crystalline phases using direct heating on a hotplate and with a femtosecond pulsed laser. Finally, we discuss the dramatic intermediate colors

seen in one of the fabricated coatings, and consider the origin of these intermediate states is discussed based on other reports in the literature. The wide gamut, large color shift and attractive appearance of these coatings paves the way for a wide range of applications, such as for security features or full-color micro-scale image writing.

2. Theory

2.1. Phase-Change Materials

A phase-change material (PCM) has two or more distinct solid phases, which exhibit a contrast in optical or electrical properties. An external signal, such as a laser or pulsed current, can be used to switch between phases, which causes the optical or electrical response of a device incorporating the PCM to change. Depending on the PCM, this change may be reversible or irreversible. The phase change should also be bistable, so the material will not spontaneously switch at room temperature.

A well-known group of PCMs are the chalcogenide PCMs, which are compounds containing chalcogens such as sulfur and tellurium. Many chalcogenide PCMs have desirable properties: high optical or electrical contrast, bistable phases, and fast, reversible switching. Most notably, the family of germanium-antimony-telluride (GST) PCMs have seen significant research interest, and are also used commercially in re-writable optical memories such as CDs and DVDs.

A typical chalcogenide PCM exhibits a change between an amorphous and a crystalline solid phase, shown in **Figure 1**. In the amorphous phase, the PCM is in a disordered, glasslike structure. It can be switched to the crystalline phase by heating above its crystallization temperature T_C, which provides enough energy for the PCM atoms to overcome the energy barrier and rearrange into an energetically favorable ordered crystalline structure. To return the PCM to its amorphous phase, it must be heated above its melting temperature T_M ($>T_C$) and then rapidly cooled (quenched) to "lock in" the disordered arrangement of the atoms.

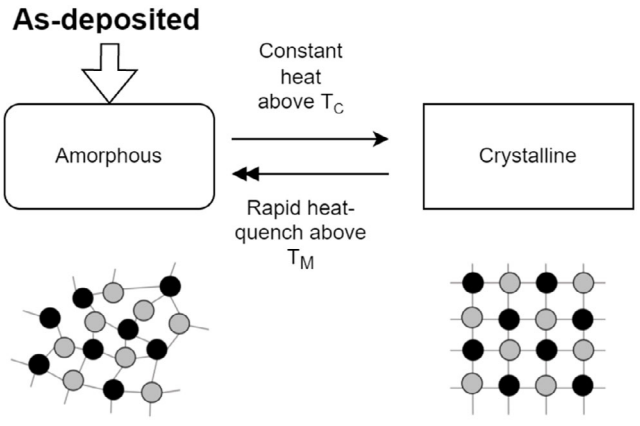

Figure 1. A flowchart schematic showing a representation of the amorphous and crystalline phases of a typical chalcogenide PCM. When deposited as a thin-film layer, the PCM is initially in its disordered amorphous phase. Crystallization may be induced by heating above the crystallization temperature T_C in order to overcome the energy barrier between the two states. The crystal phase may be re-amorphised by further heating above the melting temperature T_M (where $T_C < T_M$) followed by rapid quenching to "lock in" the disordered arrangement of the liquid state.

2.2. PCMs in Color Coatings

Recent interest in phase-change photonics has brought renewed attention onto many PCMs. Their behavior at scale and fast switching speeds has made them an attractive option for metasurfaces and photonic integrated circuits, opening up new opportunities in sensing, photonic memories, plasmonic structures, and color control.[8,9] The design of structures with large optical contrast has applications in read-write optical memory,[10] but has also seen interest for nanoscale image reproduction, low-power displays, and security features.

There are generally two main approaches for generating color in reflectance using thin films. The first is in an asymmetric Fabry–Perot cavity, which exhibits absorption bands at resonant wavelengths, leading to strong color.[11–15] A large gamut can be obtained by changing the thickness of the cavity layer, making these coatings a very versatile option to generate color. These devices are typically highly angle-dependent, although use of a higher-index cavity material mitigates this. Previous works have used a thin layer of GST[16–19] or GeTe[20] as the top layer of the cavity, due to its large absorbance. These coatings generate bright color in a range of hues, and show excellent optical contrast between phases, especially in the greyscale.[17,18] These may also be integrated with metasurfaces[21,22] to further tune the color and create an array of pixels that can be individually switched. The drawback of these coatings is a limited hue shift between phases, due to the low thickness of the GST layer and its placement in the stack. For example, a Fabry–Perot stack incorporating Al, SiO_2, and a top layer of GST was shown to generate good colors,[23] but with a limited hue shift of only $\Delta h = 45$ as defined in the CIELCh color space (see Section 2.4 for definition).

A second coating type, the so-called perfect absorber design,[24,25] typically yields a larger hue shift between phases. This coating type uses a highly reflective metallic layer with a thin lossy absorber layer to generate color. The response is highly sensitive to the index of the lossy layer, meaning that when a PCM is used, the change in phase leads to a large shift in the absorption band.[25] The drawback of this approach is that the gamut of available colors is limited. The color may be tuned by changing the thickness of the lossy layer; but increasing the thickness also adds additional absorption losses, which degrade the brightness and chroma of the color. This is especially an issue for GST and similar materials (such as GeTe), which have large absorbance in the visible spectrum.

2.3. Sb_2S_3 for Visible Photonics Applications

With the renewed interest in PCMs, many alternative materials have also seen study, including those previously rejected as viable candidates. Sb_2S_3 is an example of a PCM that has recently reemerged as a promising candidate for phase-change photonics. Its bistable phase transition was first described in the 1950s,[26] but work in the 1990s determined its phase change was irreversible

and that the material was most suited to write-once, read-many-times (WORM) memory.[27,28] However, newer works[2,3] have recently demonstrated reversible and repeatable switching of Sb_2S_3 using a pulsed laser, which opens up a wide range of new applications for this material.

Sb_2S_3 has very attractive optical properties, particularly in the visible range. **Figure 2** shows a comparison between the refractive index of GST (left) and Sb_2S_3 (right) between 380–780 nm. Compared to GST, the value of k for Sb_2S_3 is much lower in both the amorphous and the crystalline phases, leading to lower absorbance in the visible range. Meanwhile, the index contrast between the phases of Sb_2S_3 is large over the whole of the visible range. This makes Sb_2S_3 a compelling alternative to GST in the realm of visible phase-change photonics. It also has excellent switching properties, with a lifetime better than 4000 cycles.[3] Its crystallization temperature T_C is around 250°–300°,[2,4,29–31] and its melting temperature is around 550°.[32] Crystallization may be achieved using direct heating, Joule heating with a current, or laser heating; re-amorphisation may be achieved using a pulsed laser or current, which enables heating above the melting temperature followed by rapid cooling at a rate of around 1°/ns[2] to "lock in" the disordered arrangement.

Due to its excellent properties in the visible spectrum, Sb_2S_3 has seen interest for use in color coatings, particularly in the perfect-absorber type stacks. Excellent color can be obtained from a layer of Sb_2S_3 on top of an Al mirror,[2,4] with an impressive hue shift of $\Delta h = 87$, and the authors also demonstrated microscale image writing using a pulsed laser to change the phase of the Sb_2S_3 layer. However, the gamut of colors that can be obtained from this stack type is limited. A similar coating using Sb_2S_3 and Ag[6] showed an improved gamut in the green and blue region, but gave a limited hue shift between the amorphous and crystalline phases. The use of Sb_2S_3 as the cavity material in a Fabry–Perot-type stack was also shown to be possible, due to its low absorbence in the amorphous phase,[5] but the gamut of available colors was also limited in this case. Finally, a stack design with many alternating layers of SiO_2 and Sb_2S_3 has been shown to give an excellent hue shift of $\Delta h = 81$, with the possibility of generating pure blue and pure red colors;[7] however, this coating type is difficult to optimize and fabricate, due to the large number of layers with very low thickness.

In this work we suggest an alternative design, based on our previous work using an $Ag/SiO_2/Ti$ Fabry–Perot coating to generate color. In contrast to previous approaches using PCMs in this coating type, the Sb_2S_3 layer is inserted on top of the lower metallic layer to modify the cavity resonance. This combines the advantages of both the Fabry–Perot and the perfect absorber coating types. Using the Fabry–Perot structure enables a wide gamut of colors to be obtained, and placing the Sb_2S_3 layer next to the lower metallic layer exploits the sensitivity of the phase-shift on reflection between these layers to the index of the Sb_2S_3 layer. In this way, the $Ag/Sb_2S_3/SiO_2/Ti$ coating yields both a wide gamut, and an excellent hue shift between the amorphous and the crystalline phases. We also demonstrate a second design using Ag as the top layer, showing that this gives further improved color compared to using Ti.

2.4. Simulating Color and Color Shift

To assess the range of colors that could be obtained using the proposed coating design, we used simulations to predict the color of the coatings for different thicknesses of Sb_22S_3, SiO_2, and metal layers. The transfer-matrix method was employed to calculate the reflectance spectrum of the coatings over the visible range, between 380 and 780 nm. For this, we used the open-source Thin Film Toolbox,[33] a MATLAB software package designed to aid in thin-film modeling. The refractive index values for bulk Ag were taken from the SOPRA database, available at http://www.sspectra.com/sopra.html (accessed February 2022). Refractive index information Sb_22S_3 in the crystalline and amorphous states was determined experimentally (see Section 6 for more information). The refractive indices of SiO_2, Ti and thin Ag were determined in previous experimental work.[34,35] In all cases, the coating appearance was simulated at normal incidence.

To calculate the color of the coatings, we multiplied the simulated reflectance spectrum with the spectral power distribution of a CIE D65 standard illuminant.[36,37] This represents average

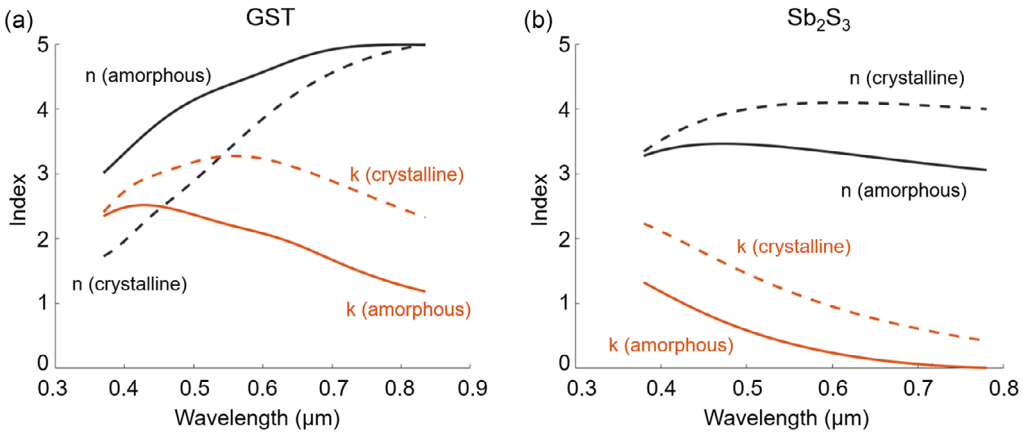

Figure 2. The refractive index n (real) and k (imaginary) of thin-film a) GST and b) Sb_2S_3, in the amorphous and crystalline states (solid, dashed). Sb_2S_3 shows comparable optical contrast to GST, and also has a consistently lower k, leading to lower absorption over the visible range. Data obtained from experimental measurements, as described in Section 6.

daylight, and was chosen to represent viewing the coatings under neutral lighting. The reflected spectrum was then converted to CIEXYZ color coordinates using the defined CIE color-matching functions,[38] which describe the color of the coating as viewed by a standard observer.

To visualize the predicted colors, we converted the XYZ coordinates to sRGB coordinates to generate color swatches. We also converted the XYZ coordinates to the CIELCh coordinate system, which is a polar representation of the CIELab coordinate system.[39] This system uses intuitive parameters to describe color: luminance L (brightness or lightness of the colors), chroma C (saturation or "strength" of the color), and hue h (represented as an angle, with red at 0° and green at 180°). In this coordinate system, the hue shift Δh gives a close match to the perceived difference between hues.

The hue shift is given by the length of the chord between two colors $L_1C_1h_1$ and $L_2C_2h_2$

$$\Delta h = \sqrt{\Delta E^2 - \Delta L^2 - \Delta C^2} \tag{1}$$

where $\Delta L = L_1 - L_2$, $\Delta C = C_1 - C_2$ and ΔE is the total color difference given by the Euclidean distance between the two points ($= \sqrt{\Delta L^2 + \Delta a^2 + \Delta b^2}$ in CIELab). Δh is larger when the chroma C of both colors is high and when there is a large hue angle difference between them.

3. Results

3.1. Simulated Color Coatings with Sb_2S_3 Layer

Two stack types were investigated in this work: Ag/Sb_2S_3/SiO_2/Ti, and Ag/Sb_2S_3/SiO_2/Ag. Simulations were used to assess the range of colors that could be achieved for different thicknesses of the Sb_2S_3 and SiO_2 layers, with the goal of demonstrating a wide gamut, high chroma, and a large hue shift Δh between the amorphous and crystalline phases.

Figure 3 shows the results of the simulations for the coatings using Ti (left) or Ag (right) as the top layer. The gamuts demonstrate the range of colors obtained for different thicknesses of the SiO_2 cavity layer, without a layer of Sb_2S_3 (top) or with 10, 30, 50 or 200 nm of Sb_2S_3 (descending). The insets at the bottom show selected combinations of SiO_2 and Sb_2S_3 thickness, which exhibit a large color change between the amorphous (a) and crystalline (c) phases.

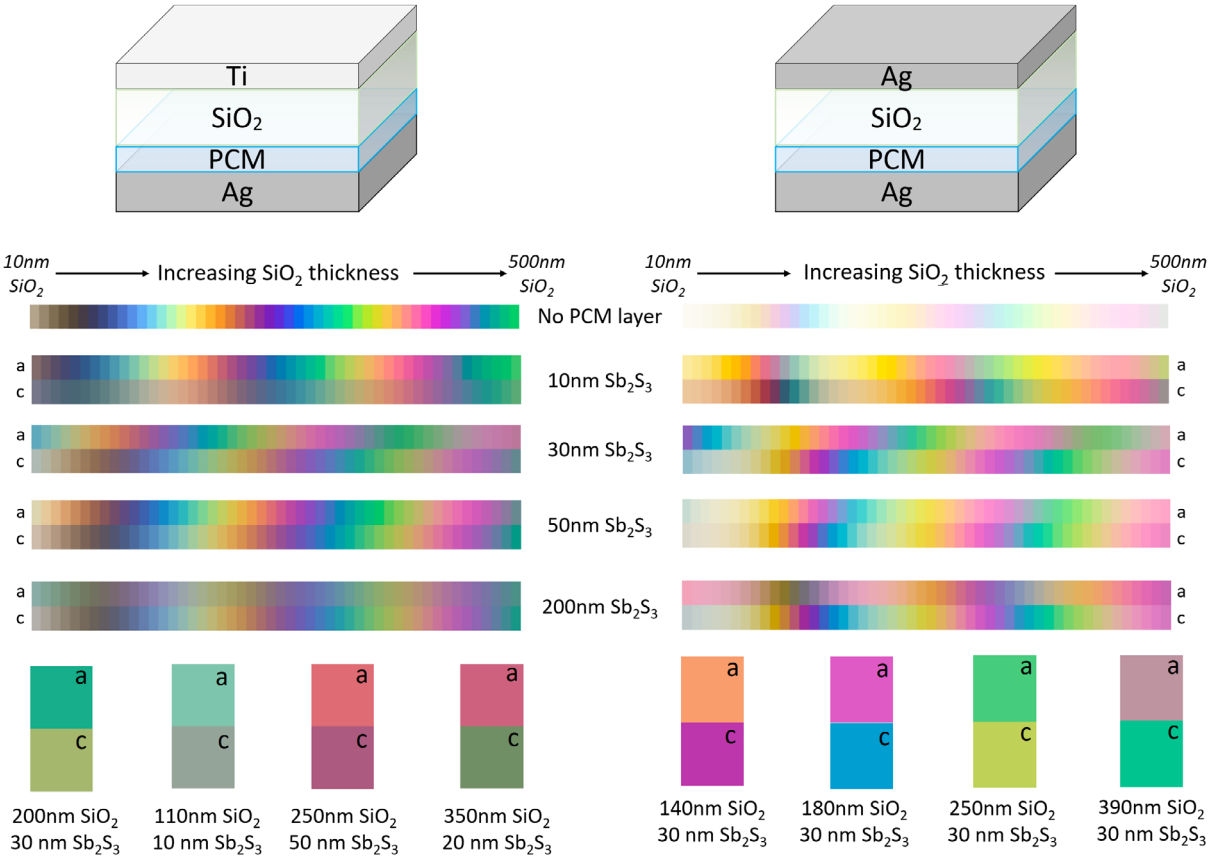

Figure 3. The range of colors that can be obtained by adding a layer of Sb_2S_3 into a metal-dielectric-metal coating using either 10 nm Ti (left) or 10 nm Ag (right) as the top layer. Insets (below) show selected amorphous (a) and crystalline (c) color pairs for certain combinations of SiO_2 and Sb_2S_3 thickness. For the stack with Ti, increasing the Sb_2S_3 thickness significantly decreases the brightness and chroma of the colors, due to absorption losses. Conversely, for the stack with Ag, a layer of 30–50 nm Sb_2S_3 the chroma of the resulting colors, leading to coatings with excellent brightness and large color contrast between the amorphous and crystalline phases.

3.1.1. Simulated Coatings with Ti

When Ti is used as the top layer of the coating, it was found that the optimal Sb_2S_3 thickness to generate a large hue shift was between 20 and 30 nm. As seen in Figure 3, left, introducing a layer of 30 nm Sb_2S_3 produces a significant hue shift between the amorphous and crystalline phases. A coating with 200 nm SiO_2 and 30 nm Sb_2S_3 (inset, left) gives a vibrant teal color in the amorphous phase, shifting to a bright yellow-green color in the crystalline phase.

However, the Sb_2S_3 layer also introduces additional absorption losses to the cavity, causing the overall chroma of the colors to be reduced compared to the coating with no Sb_2S_3 layer. Increasing the layer thickness to 50 nm and then 200 nm also increases the absorption losses, which causes the colors to become even darker with lower chroma. On the contrary, decreasing the Sb_2S_3 layer thickness to only 10 nm improves the chroma in the amorphous phase, but significantly reduces the hue shift between the amorphous and crystalline phases. As such, the optimal thickness of Sb_2S_3 was determined to be between 20 and 30 nm to generate the largest possible hue shift.

For this coating, the optimal hue shift was found to be given by a coating with 350 nm SiO_2 and 20 nm Sb_2S_3. The resulting color is shown in the bottom right inset, with a magenta color in the amorphous phase and a green color in the crystalline phase. The hue shift of this coating was $\Delta h = 63$. This coating design was selected for experimental deposition and annealing using a hotplate, which is described in Section 3.2.1.

3.1.2. Coatings Using Ag

When Ag is used as the top layer of the coating (Figure 3, left), the colors obtained without a layer of Sb_2S_3 are very pale, close to white. This is because the absorption band of the cavity is very narrow, as Ag is close to an ideal reflector ($n \ll k$). When a layer of Sb_2S_3 is introduced, it adds absorption losses into the cavity and significantly widens the absorption band, which increases the chroma of the resulting colors.

As before, a layer of only 10 nm Sb_2S_3 is insufficient to give a large hue shift between the amorphous and the crystalline phases. When the thickness is increased to 30 nm, a large hue shift is seen between the amorphous and crystalline phases of the layer. In addition, the colors are much brighter than those seen with a Ti top layer, due to the lower absorption losses overall. Increasing the Sb_2S_3 layer thickness further does not increase the hue shift between phases, and for very thick layers of 200 nm the chroma in the amorphous phase is reduced.

For these coatings, the optimal Sb_2S_3 thickness was found to be 30 nm. Several coating designs are shown in insets below, with especially large hue shifts of $\Delta h = 78$ for the orange-purple coating (first inset, 140 nm SiO_2) and $\Delta h = 74$ for the magenta-blue coating (second inset, 180 nm SiO_2). Along with a large hue shift, the colors also display an excellent brightness and high chroma.

The coating design with 140 nm SiO_2 was chosen for deposition, as it had the highest hue shift. The coating design with 250 nm SiO_2 (green-gold, third inset) was also chosen for deposition, to demonstrate the range of colors that could be achieved from these coatings. The phase change of these coatings was explored using laser writing, detailed in Section 3.2.2.

3.2. Experimental Deposition

3.2.1. Ti Coating and Hotplate Annealing

The optimized Ti coating design with 20 nm Sb_2S_3 and 350 nm SiO_2 was deposited onto the unpolished side of single-side polished 1" Si test wafers. **Figure 4**a shows a schematic of the coating design. The thickness of the lower Ag layer was 150 nm, and a 5 nm layer of Cr was deposited between the substrate and the Ag layer to aid adhesion. Additionally, a top layer of 26 nm SiO_2 was deposited on top of the Ti layer to prevent oxidation, and a 26 nm SiO_2 barrier layer was deposited between the Ag layer and the Sb_2S_3 layer to prevent diffusion (as reported in[2,40]). Therefore, the final coating design was 5 nm Cr/150 nm Ag/2.6 nm SiO_2/20 nm Sb_2S_3/350 nm SiO_2/10 nm Ti/26 nm SiO_2. Further information on the deposition parameters is described in Section 6.

Figure 4b shows the simulated reflectance spectra when the Sb_2S_3 layer is in the amorphous and crystalline phases. When the phase changes from amorphous to crystalline, the reflectance spectrum is shifted toward longer wavelengths. The amplitude of the rightmost peak in the spectrum is also lower in the crystalline phase, due to the larger absorbance of Sb_2S_3 in the crystalline phase. These changes cause the color of the coating to shift from magenta in the amorphous phase to green in the crystalline phase.

After deposition, some samples were annealed using a hotplate at 300 °C to change the phase of the Sb_2S_3 layer from amorphous to crystalline. Figure 4c shows a photograph of the coating on samples at various stages of crystallization, after heating for different lengths of time. The as-deposited coating (left) is in the amorphous phase, and shows a magenta color similar to that predicted by simulations. The sample on the right was heated until the color stabilized (suggesting complete crystallization), which took approximately two minutes. Further heating over one hour did not produce any further color change. This sample shows a green color, which also gives a good match to the simulation.

In between the fully amorphous and fully crystalline states, the sample was seen to progress through a range of intermediate colors when placed on the hotplate: first purple, then dark blue, followed by lighter blue-green, finally settling at the green color of the fully crystallized samples. The blue sample in the center of the photograph represents one of these intermediate states, seen after around 30 s of annealing on the hotplate. The possibility of intermediate crystallization states is investigated further in Section 4.1.

3.2.2. Ag Coating and Laser Annealing

Two coatings with an Ag top layer were deposited on the unpolished side of single-side polished 1" Si test wafers. **Figure 5** shows schematics of the two coatings: (a), a coating with 140 nm SiO_2 with an optimized hue shift (orange-purple); and (b), a coating with 250 nm SiO_2, chosen to demonstrate two additional colors possible with this stack type (green-gold). As before, an adhesive

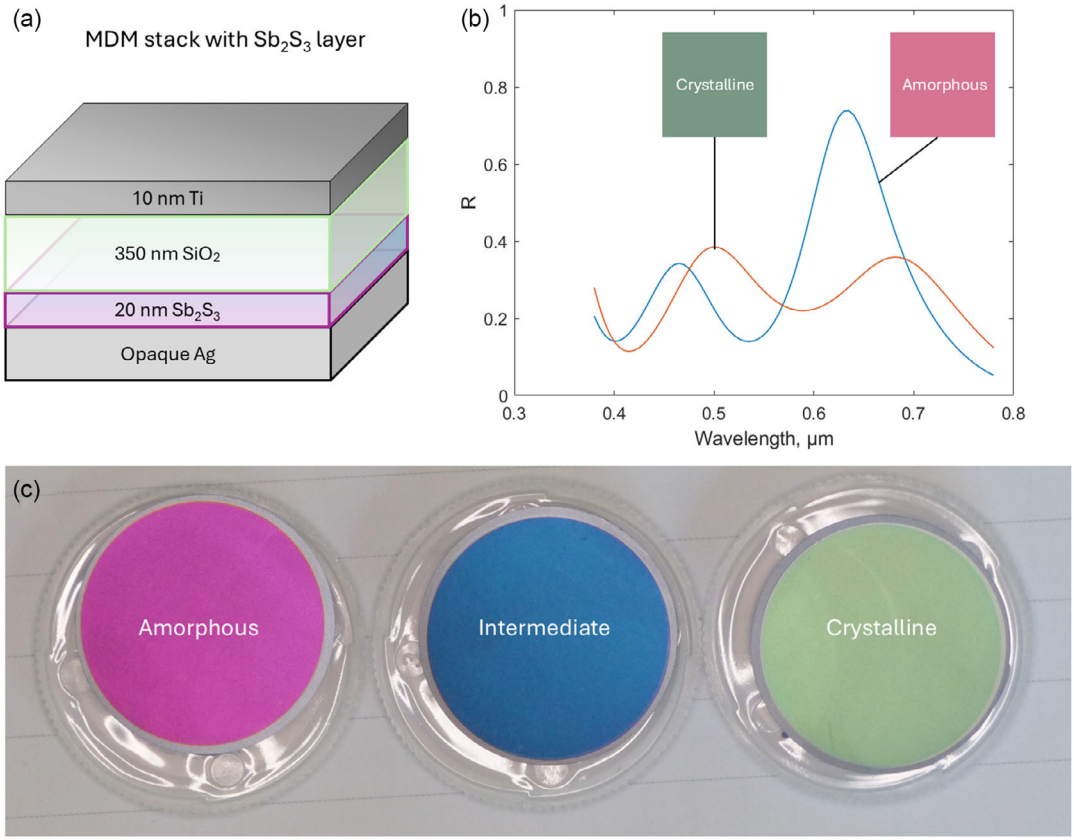

Figure 4. a) Schematic of an MDM stack with opaque Ag, 350 nm SiO_2 and 10 nm Ti, incorporating a 20 nm Sb_2S_3 layer. b) The simulated reflectance of this stack in the amorphous and crystalline phases, and the resulting color under a D65 illuminant. The stack exhibits a large hue shift, from magenta in the amorphous phase to green in the crystalline phase. c) Photographs of the coating deposited on 1" Si wafers (with additional adhesive and protective layers, as described in Section 3.2.1). Left: the as-deposited coating in the amorphous phase, showing a magenta color. Middle: the coating after hotplate annealing for thirty seconds, leading to partial crystallization and a deep blue color. Right: the coating after full crystallization via hotplate annealing, showing a green color.

layer of Cr was used, along with additional barrier layers of SiO_2. The final coating recipes were 5 nm Cr/150 nm Ag/2.6 nm SiO_2/30 nm Sb_2S_3/140 nm SiO_2/10 nm Ag/26 nm SiO_2 for the orange-purple coating, and 5 nm Cr/150 nm Ag/2.6 nm SiO_2/30 nm Sb_2S_3/250 nm SiO_2/10 nm Ag/26 nm SiO_2 for the green-gold coating.

The plots in Figure 5c,d show the reflectance spectra of the coatings. Both coatings show relatively narrow absorption bands with wide reflection peaks compared to the coating using Ti as the top layer (Figure 4). This contributes to the brighter colors obtained from these coatings. When the Sb_2S_3 phase changes from crystalline to amorphous, the reflection spectrum becomes redshifted for both coatings, with the peaks and troughs of the spectrum shifting to longer wavelengths. This effect is more prominent at longer wavelengths, where the index contrast between the phases of Sb_2S_3 is greater. The reflectance peaks are also slightly lower in the crystalline phase, especially at longer wavelengths, owing to the greater absorption of crystalline Sb_2S_3.

After deposition, these coatings were exposed to a 1030 nm laser to induce crystallization in selected areas (see Section 6 for more information). Photographs of the laser-annealed coatings are shown in **Figure 6**, with (a) and (c) showing the orange-purple coating and (b) and (d) showing the green-gold coating. In (a) and (b), the squares were etched using increasing laser energy from 0.2 to 1.9 μJ to demonstrate control over intermediate phases of crystallization. In (c) and (d), the laser was used to selectively etch certain areas of the sample, creating the letters "FR". This demonstrates that both the degree and location of crystallization can be finely controlled using a laser.

4. Discussion

Simulations have shown that Fabry–Perot coatings incorporating Sb_2S_3 can be used to generate a wide gamut of colors, which have a large hue shift between phases while preserving high chroma. When deposited, these coatings showed good agreement with the predicted results from simulation, yielding bright and saturated colors. It was also demonstrated that these coatings could be switched from the amorphous to the crystalline phase using either heating on a hotplate, or etching using a pulsed laser.

The success of selective switching using a laser has particular interest for applications such as microscale image writing, security features, or low-powered displays. However, a key drawback of the

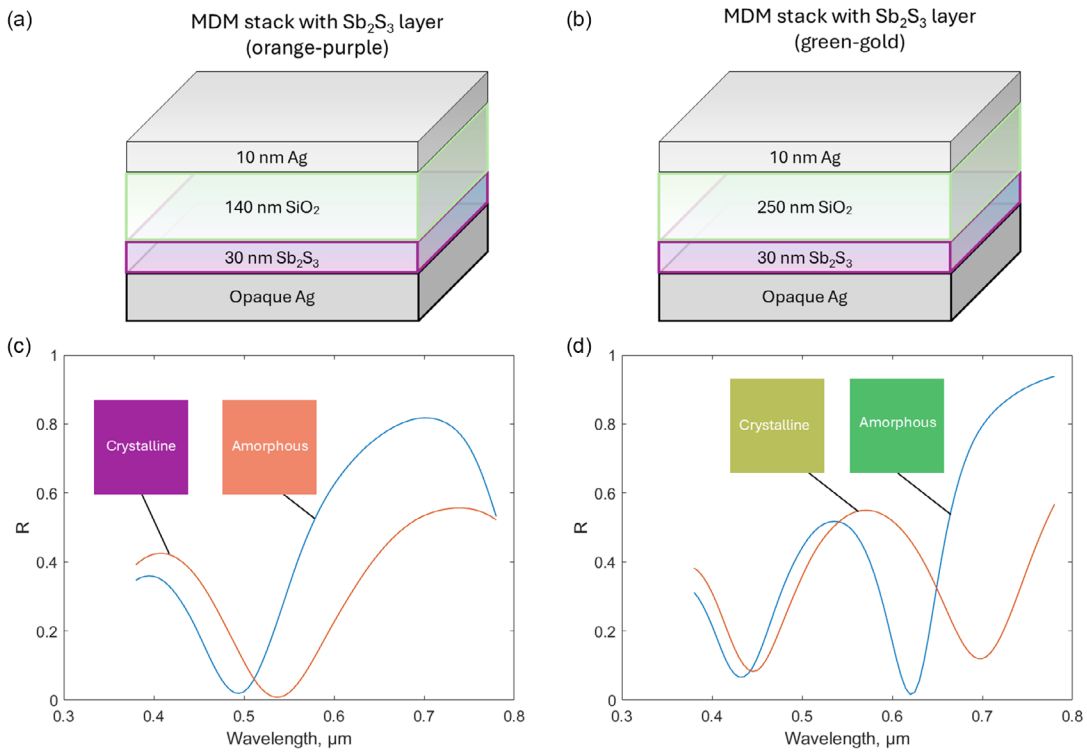

Figure 5. Two PCM-MDM stack designs with a large hue shift between the amorphous and crystalline PCM phases, which were chosen for deposition. a) A stack with 30 nm Sb_2S_3, 140 nm SiO_2, and 10 nm Ag. The spectrum in c) reveals the color of the coating as observed under a D65 illuminant, showing that the coating changes from an orange color to a deep magenta color when the Sb_2S_3 layer changes from amorphous to crystalline. b) A stack with 30 nm Sb_2S_3, 250 nm SiO_2, and 10 nm Ag. The spectrum in d) shows that the coating changes from a green color in the amorphous state to a yellow color in the crystalline state, when viewed under a D65 illuminant.

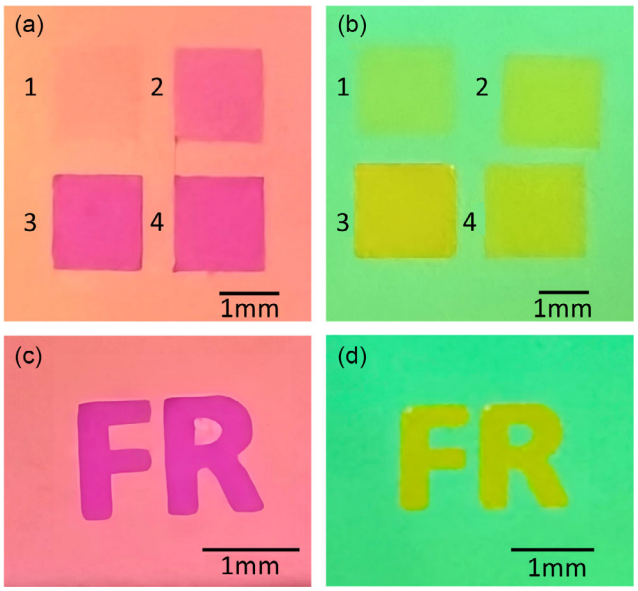

Figure 6. Photographs of laser writing on the two coating designs shown in Figure 5. a,c) show the orange-purple coating, and b,d) show the green-gold coating. In (a) and (b), the squares 1-4 were annealed with increasing laser energy: 0.2, 0.5, 1.0, and 1.9 μJ, respectively. A gradual change in color is seen from fully amorphous to fully crystallized, showing the intermediate annealing states that can be accessed at different laser energies. In (c) and (d), the letters "FR" were etched at a laser energy of 1.9 μJ.

laser switching approach is limited scalability to large areas. While addressing a manufacturing challenge like this is beyond the scope of this work, it is a hurdle that needs to be overcome for future development and implementation of these coatings.

Both methods of annealing also show the ability to access intermediate states for the Sb_2S_3 layer. For laser annealing, a laser power below 1.9 μJ yielded an intermediate color appearance, indicating that the degree of crystallization might depend on the laser power. For hotplate annealing, the sample shown in Figure 4 showed a spectacular shift in color during the heating process, progressing from the initial magenta to dark purple, deep blue, cyan, and finally green after ≈2 min. The vivid appearance of the intermediate colors was particularly intriguing. Below, we discuss previous work investigating the formation of intermediate amorphous-crystalline states for Sb_2S_3, and compare to our own experimental results.

4.1. Intermediate States - Bilayer versus Domain-Driven Model

The intermediate colors seen here have also been shown in other works. Liu et al.[4] demonstrated image writing using a pulsed laser to re-amorphise an Sb_2S_3 layer. By tuning the laser power, they were able to access a range of colorscolors between the fully crystalline and the fully-amorphous states. These results appear similar to the range of colors we observed using laser writing (Figure 6).

The mechanics of a hybrid crystalline-amorphous layer were further investigated by Gao et al.[41] Their work found that the optical properties of partially re-amorphised Sb_2S_3 films were consistent with a bilayer model, where upon irradiation with a small number of pulses, the upper part of the Sb_2S_3 layer was amorphised but the lower part of the layer remained in the crystalline phase. By selectively tailoring the pulse power and number of pulses, the degree of amorphisation could be controlled from 0 to 100%.

Conversely, Parize et al.[42] showed that the opposite transition—amorphous to crystalline—appeared to be mostly domain-driven. Raman scattering and X-ray diffraction of Sb_2S_3 films during crystallization showed the formation of coarse grains at temperatures between 260° and 290°, with an intermediate metallic Sb phase. When the temperature was raised to 300°, diffusion occurred, leading to large pyramidal clusters at the surface of the film. These results indicate that a partially crystallized layer may be in an inhomogeneous intermediate state, and that the nature of this intermediate state depends on the crystallization process (which itself depends on temperature, environment, and so on).

We implemented two models to attempt to describe intermediate states. The first assumed a bilayer formation, with crystalline Sb_2S_3 forming at the lower interface with the substrate (the direction of heat transfer) while the upper interface remained amorphous. The second assumed an effective layer with an intermediate index that was interpolated smoothly between the amorphous and crystalline states. The simulated colors for each intermediate-state model are shown in **Figure 7**.

The smooth color transition seen here matches well with the intermediate color changes seen for the laser etching. However, neither model appears to be able to explain the blue appearance of the intermediate states obtained from hotplate annealing. Instead, both models predict an intermediate state of a dull reddish-brown color, which smoothly transitions between magenta and green with no blue hues. This suggests that our simulations may not be a good fit for the actual behavior of the coating during hotplate annealing, and there may be other effects present when the Sb_2S_3 layer is heat-treated that these models cannot explain.

4.1.1. Layer Diffusion at Metal-Chalcogenide Interface

A possible explanation for the strange behavior of the Sb_2S_3 layer is diffusion at the Ag-Sb_2S_3 interface. Although a barrier layer was used (of 2.6 nm SiO_2), it is possible that this layer thickness was insufficient to prevent diffusion, especially when the layer was heated for several tens of seconds on the hotplate. Notably, unexpected intermediate colors were not seen for the laser-annealed samples, where the annealing time was much lower (100 µs), which may suggest that different behavior is seen over longer timescales.

Diffusion of chalcogenide layers at the interface with plasmonic metals (such as Al and Ag) is a known issue.[40] Previous works depositing Sb_2S_3 over Al[2,4] use a 5 nm barrier layer of Si_3N_4 between the layers in order to prevent diffusion. It is possible that the thinner layer we used (2.6 nm, to minimize the impact on color) or the material choice (SiO_2, rather than the more commonly used Si_3N_4 or TiN) made it insufficient to completely prevent diffusion.

In general, the behavior of metal doping in chalcogenide layers is fairly complex,[43] with many compounds that may be formed. The possible diffusion of O molecules from the SiO_2 layer further complicates the analysis, as both Ag and Sb_2S_3 will

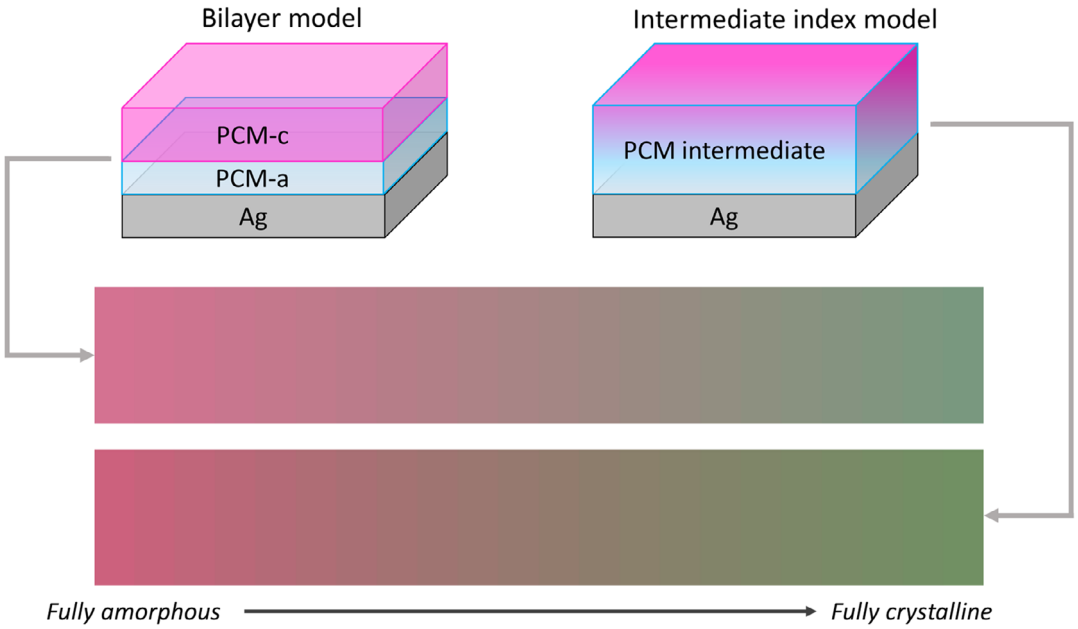

Figure 7. Simulations of the intermediate colors of the stack described in Figure 4 for two models of intermediate crystallization: top, a bilayer model, with crystallized Sb_2S_3 growing at the top of the layer (see schematic, left); bottom, a domain-driven model, with the intermediate layer assumed to have an effective index smoothly interpolated between the amorphous and crystalline states (see schematic, right). Both models show a very similar gradient in colors, from magenta to a dull brown-gray color to green.

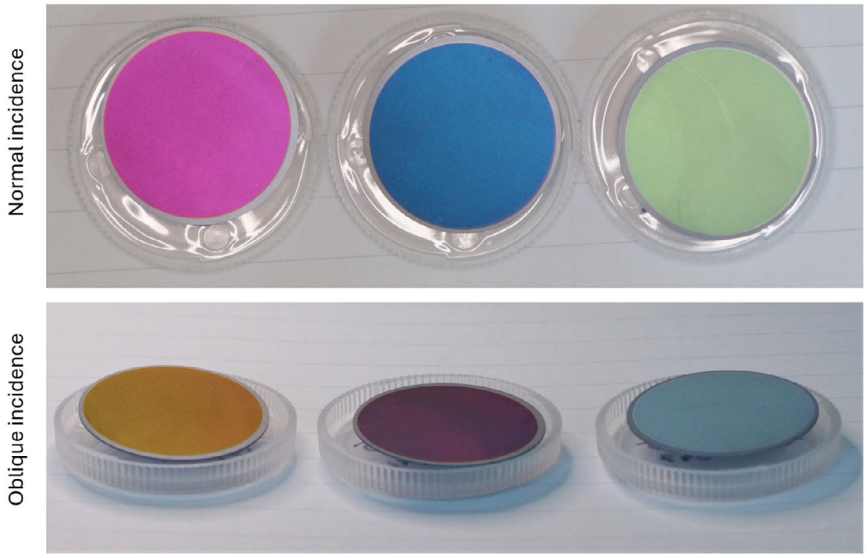

Figure 8. Appearance of the coatings shown in Figure 4, at normal incidence (top) and oblique incidence (bottom). The reflectance spectra are blueshifted at higher angle, causing the following color changes: magenta → yellow; blue → magenta; green → blue.

readily form oxides (the latter when heated at or above 300° in an oxygen-rich environment[42]).

Dong et al. (2016)[44] report that doping of Ag atoms into an Sb_2S_3 layer significantly reduces its crystallization temperature and increases crystallization speed. The optical bandgap edge is expected to be redshifted, along with a slight increase in the real part of the refractive index. Diliegros-Godines et al.[45] report a narrowing in the bandgap of Ag-doped Sb_2S_3 from 1.75 to 1.66 eV, and a red-shift of the bandgap edge from 750 to 800 nm.

This change in refractive index due to diffusion of Ag atoms could explain the blue appearance of the coatings midway through annealing. A blue appearance would indicate a high prominence of the reflectance peak around 450 nm (blue-range light), alongside suppression of the reflectance peak above 600 nm (red-range light). If this is due to photodiffusion of Ag into the Sb_2S_3 layer, then this change should, in theory, be irreversible. This could be tested by using a pulsed laser to attempt to re-amorphise the layer, as reported in.[4,41] If the original magenta color of the coating could be recovered, then that suggests the color change is due to the reversible amorphous/crystalline phase change. If the coating appearance remains different, then it suggests an irreversible diffusion of Ag atoms into the Sb_2S_3. Other investigative methods, such as secondary ion mass spectrometry (SIMS) or energy-dispersive X-ray spectroscopy (EDS), could also be used to confirm this hypothesis. Further testing of this stack is needed to determine the nature of this color change.

4.2. Angle-Dependent Behavior of Coatings

In this work, all results for the coating designs (simulated and experimental) have been shown at normal incidence. However, the behavior of Fabry–Perot-type coatings is strongly angle-dependent. When viewed at oblique angles, the reflection spectrum becomes blueshifted, leading to a significant change in color. **Figure 8** shows the coating design presented in Figure 4, photographed at normal incidence (a) and oblique incidence (≈45°) (b). The color of the coating shifts at all three phases; the magenta coating becomes yellow, the blue coating becomes magenta, and the green coating becomes blue.

For applications such as security features, strongly angle-dependent behavior can strengthen the uniqueness of the coating, as it is hard to replicate through other mediums. On the contrary, for applications like low-powered displays, angle-dependent behavior may be undesirable. In this case, use of a dielectric material with a high refractive index, for example, TiO_2, can effectively mitigate the change in reflected spectrum with angle.[1]

5. Conclusion

An active color-shift coating design incorporating the phase-change material Sb_2S_3 into a Fabry–Perot cavity has been demonstrated. Simulations were used to assess the gamut and hue shift for coatings using Ag, Sb_2S_3 and SiO_2, with either Ag or Ti as the top metallic layer. It was found that both options produced a wide gamut of colors with high chroma and brightness, with a large hue shift between amorphous and crystalline phases for an optimal thickness of Sb_2S_3.

Three coating designs with large hue shifts were chosen for deposition, and good agreement was seen between the experimental and simulated colors. The phase change of the Sb_2S_3 layer was demonstrated using either a hotplate or a pulsed laser. For both approaches, intermediate colors were achieved by restricting the heating time or the laser power, respectively. This shows the key advantage of a coating with a large hue shift, in that a wide range of colors can be obtained from a fixed coating design by changing the degree of amorphisation or crystallization. Possible applications for these coatings include luxury items, microscale image writing, as well as low-powered displays

and security features (for example, on passports or bank notes). However, further development of manufacturing approaches is needed to overcome issues of scalability in laser switching.

Hotplate annealing of one coating design showed a particularly large range of colors, from magenta in the as-deposited amorphous state, to blue, to green in the fully annealed crystalline state. The intermediate blue color was striking, as it did not match the predicted behavior from simulations. Two models were used to simulate intermediate phases of the Sb_2S_3 layer (bilayer formation, and intermediate-state crystallization), and both predicted a range of intermediate reddish-brown colors, rather than the vivid blue seen in experiments. One suggested explanation is potential diffusion between the Ag and Sb_2S_3 (as Ag-doped Sb_2S_3 is known to have different optical properties that could lead to different colors). Further testing of the coating, such as testing the reversability of the amorphous → crystalline phase change or by investigation of the Sb_2S_3 layer using suitable spectrometry or spectroscopy techniques, could provide insight into this.

6. Experimental Section

Deposition of Thin-Film Coatings: The thin-film layers in this work were deposited using electron beam evaporation in one of two Bühler-Leybold SyrusPRO 710 vacuum deposition machines. In order to prevent contamination of the material layers, one machine was used to deposit Sb_2S_3, and the other was used to deposit the remaining materials (Cr, Ag, SiO_2, and Ti). High-purity evaporation materials were provided by CODEX International.

Deposition was carried out under a vacuum of $\approx 5 \times 10^{-7}$ mbars. Coatings were deposited on rough (unpolished) surfaces in order to aid adhesion and improve the visual appearance of the resulting color. The hotplate-annealed samples in Figure 4 were deposited on the unpolished side of single-side polished 1" Si wafers, and the laser-annealed samples in Figure 6 were deposited on 1" ground glass slides. The layer thickness was monitored using a quartz balance. The deposition rate was 0.5 nm s^{-1} for SiO_2 and Sb_2S_3, 0.1 nm s^{-1} for Ag, and 0.05 nm s^{-1} for Ti.

Index Determination of GST and Sb_2S_3 Layers: For index characterization, 30 nm thick layers of GST and 70 nm layers of Sb_2S_3 were deposited on polished B270 glass slides. Measurements of reflectance and transmittance were taken using a Perkin-Elmer Lambda1050 spectrophotometer, between 380 and 780 nm. A protective layer of 10 nm SiO_2 was deposited on top of the Sb_2S_3 layers to protect from oxidation during annealing.

These measurements were used to fit the refractive index using a Tauc-Lorentz model with an Urbach tail term in the imaginary part. Fitting was performed using a custom MATLAB script incorporating the built-in global optimization function GlobalSearch.[46]

As-deposited, the films were in the amorphous phase. Measurements of the crystalline phase were obtained by annealing the samples on a hotplate to crystallize them (see below).

Hotplate Annealing: An electric hotplate was used to anneal samples containing layers of phase-change materials. The hotplate was heated to a steady temperature of 300°, and samples were placed directly on its surface to anneal. The annealing was performed in air. Annealing time was judged by eye via observing when the color change appeared to be stable, which took about 2 min for both Sb_2S_3 and GST. Additionally, almost no difference in reflectance and transmittance was measured between samples that were annealed for 2 and 30 min.

Laser Annealing: Laser annealing was performed using a 1030 nm wavelength, 400 fs pulse duration laser, with a repetition rate of 200 kHz and a 1 ms exposure time. A 20 cm converging lens was used to focus the laser to a spot size of 75 μm ($1/e^2$). Laser scanning was performed by mounting the sample on a motion stage at the focal plane of the laser. Both the laser and the motion stage were controlled using LabVIEW in order to synchronize exposure with the motion during scans. During scans, each spot was exposed for 100 ms, with a 65 μm step size between spots (leading to a 13% spot-to-spot overlap). The laser power was varied between 0.2 μJ and 1.9 μJ (95% power). For the chosen exposure time, a more dramatic change in color is seen as the laser power increases (Figure 6), showing that the laser power can be used to control the degree of crystallization. which was scanned over the surface by mounting the sample on a motion stage controlled via LabVIEW.

Acknowledgements

This work was supported by SATT South-East as a technology maturation project.

Conflict of Interest

The authors declare no conflict of interest.

Data Availability Statement

The data that support the findings of this study are available from the corresponding author upon reasonable request.

Keywords

active color, color coatings, phase-shift materials, Sb_2S_3, thin-film coatings

Received: November 18, 2024
Revised: June 5, 2025
Published online:

[1] R. Shurvinton, F. Lemarchand, A. Moreau, J. Lumeau, *Adv. Photonics Res.* **2022**, *3*, 2200102.
[2] W. Dong, H. Liu, J. K. Behera, L. Lu, R. J. H. Ng, K. V. Sreekanth, X. Zhou, J. K. W. Yang, R. E. Simpson, *Adv. Funct. Mater.* **2019**, *29*, 1806181.
[3] M. Delaney, I. Zeimpekis, D. Lawson, D. W. Hewak, O. L. Muskens, *Adv. Funct. Mater.* **2020**, *30*, 36.
[4] H. Liu, W. Dong, H. Wang, L. Lu, Q. Ruan, Y. S. Tan, R. E. Simpson, J. K. W. Yang, *Science Advances*, Vol. *6*, American Association for the Advancement of Science, Washington, USA **2020**, p. eabb7171.
[5] K. V. Sreekanth, R. Medwal, Y. K. Srivastava, M. Manjappa, R. S. Rawat, R. Singh, *Nano Lett.* **2021**, *21*, 10070.
[6] D. T. Yimam, M. Liang, J. Ye, B. J. Kooi, *Adv. Mater.* **2024**, *36*, 2303502.
[7] S. Jana, K. V. Sreekanth, O. A. M. Abdelraouf, R. Lin, H. Liu, J. Teng, R. Singh, *Nano Letters* **2024**, *24*, 3922.
[8] M. Wuttig, H. Bhaskaran, T. Taubner, *Nature Photonics*, Vol. *11*, Springer Nature, Berlin, Germany **2017**.
[9] S. Abdollahramezani, O. Hemmatyar, H. Taghinejad, A. Krasnok, Y. Kiarashinejad, M. Zandehshahvar, A. Alù, A. Adibi, *Nanophotonics*, Vol. *9*, De Gruyter **2020**, p. 1189.
[10] F. F. Schlich, P. Zalden, A. M. Lindenberg, R. Spolenak, *ACS Photonics* **2015**, *2*, 178.
[11] C.-S. Park, V. R. Shrestha, S.-S. Lee, D.-Y. Choi, *Sci. Rep.* **2016**, *6*, 25496.
[12] S. S. Mirshafieyan, T. S. Luk, J. Guo, *Opt. Mater. Express* **2016**, *6*, 4.
[13] H. Song, L. Guo, Z. Liu, K. Liu, X. Zeng, D. Ji, N. Zhang, H. Hu, S. Jiang, Q. Gan, *Adv. Mater.* **2014**, *26*, 2737.

[14] J. Kim, H. Oh, M. Seo, M. Lee, *ACS Photonics* **2019**, *6*, 2342.
[15] M. A. Kats, S. J. Byrnes, R. Blanchard, M. Kolle, P. Genevet, *Appl. Phys. Lett.* **2013**, *103*, 101.
[16] S. Yoo, T. Gwon, T. Eom, S. Kim, C. S. Hwang, *ACS Photonics*, Vol. *3*, American Chemical Society, Washington, USA **2016**, p. 1265.
[17] P. Hosseini, C. D. Wright, H. Bhaskaran, *Nature* **2014**, *511*, 206.
[18] C. Ríos, P. Hosseini, R. A. Taylor, H. Bhaskaran, *Adv. Mater.* **2016**, *28*, 4720.
[19] S. Cueff, A. Taute, A. Bourgade, J. Lumeau, S. Monfray, Q. Song, P. Genevet, B. Devif, X. Letartre, L. Berguiga, *Adv. Opt. Mater.* **2021**, *9*, 2001291.
[20] M. Jafari, L. J. Guo, M. Rais-Zadeh, *Adv. Opt. Mater.* **2019**, *7*, 1801214.
[21] S. G.-C. Carrillo, L. Trimby, Y.-Y. Au, V. K. Nagareddy, G. Rodriguez-Hernandez, P. Hosseini, C. Ríos, H. Bhaskaran, C. D. Wright, *Adv. Opt. Mater.* **2019**, *7*, 1801782.
[22] S. Luo, Z. Zhang, X. He, Z. Zhang, X. Li, M. Fu, J. Yang, *Photonics* **2023**, *10*, 7.
[23] F. Liu, H. Shi, X. Zhu, P. Dai, Z. Lin, Y. Long, Z. Xie, Y. Zhou, *Appl. Opt.* **2018**, *57*, 9040.
[24] M. A. Kats, D. Sharma, J. Lin, P. Genevet, R. Blanchard, Z. Yang, M. M. Qazilbash, D. N. Basov, S. Ramanathan, F. Capasso, *Applied Physics Letters*, Vol. *101*, American Institute of Physics, Maryland, USA **2012**, p. 221101.
[25] M. A. Kats, R. Blanchard, P. Genevet, F. Capasso, *Nat. Mater.* **2013**, *12*, 20.
[26] L. Gildart, *J. Non-Cryst. Solids* **1970**, *2*, 240, proceedings of the Symposium on Semiconductor Effects in Amorphous Solids.
[27] P. Arun, A. G. Vedeshwar, N. C. Mehra, *J. Phys. D: Appl. Phys.* **1999**, *32*, 183.
[28] P. Arun, A. G. Vedeshwar, *J. Non-Cryst. Solids* **1997**, *220*, 63.
[29] F. Perales, G. Lifante, F. Agulló-Rueda, C. de las Heras, *J. Phys. D: Appl. Phys.* **2007**, *40*, 2440.
[30] B. Krishnan, A. Arato, E. Cardenas, T. K. D. Roy, G. A. Castillo, *Appl. Surf. Sci.* **2008**, *254*, 3200.
[31] A. D. DeAngelis, K. C. Kemp, N. Gaillard, K. S. Kim, *ACS Applied Materials & Interfaces*, Vol. *8*, American Chemical Society, Washington, USA **2016**, p. 8445.
[32] *CRC Handbook of Chemistry and Physics*, (Ed: W. M. Haynes), CRC Press, Boca Raton, Florida, USA **2017**, pp. 4–48.
[33] U. Griesmann, Thin film toolbox, https://sites.google.com/site/ulfgri/numerical/thin-films, (accessed: December 2019).
[34] R. Shurvinton, F. Lemarchand, A. Moreau, J. Lumeau, *J. Eur. Opt. Soc.-Rapid Publ.* **2021**, *17*, 29.
[35] R. Shurvinton, V. Allard, A. Lereu, A. Moreau, F. Lemarchand, J. Lumeau, *J. Eur. Opt. Society-Rapid Publ.* **2024**, *20*, 8.
[36] *Colorimetry - Part 2: CIE Standard Illuminants, Standard*, Commission Internationale de L'Eclairage, Vienna, Austria **2022**.
[37] I. C. on Illumination (CIE), Cie standard illuminant D65 **2019**, https://doi.org/10.25039/CIE.DS.hjfjmt59, (accessed: 2020).
[38] Proceedings of the Commission Internationale de L'Eclairage, 8th Session, CIE, Cambridge University Press, Cambridge University Press and Assessment, Shaftesbury Road, Cambridge, CB2 8EA UK **1931**.
[39] D. Malacara, *Color Vision and Colorimetry: Theory and Applications*, 2nd ed., SPIE Press, Bellingham, Washington, USA **2011**.
[40] L. Lu, W. Dong, J. K. Behera, L. Chew, R. E. Simpson, *J. Mater. Sci.* **2019**, *54*, 2814.
[41] K. Gao, K. Du, S. Tian, H. Wang, L. Zhang, Y. Guo, B. Luo, W. Zhang, T. Mei, *Adv. Funct. Mater.* **2021**, *31*, 2103327.
[42] R. Parize, T. Cossuet, O. Chaix-Pluchery, H. Roussel, E. Appert, V. Consonni, *Mater. Des.* **2017**, *121*, 1.
[43] M. Frumar, T. Wagner, *Curr. Opin. Solid State Mater. Sci.* **2003**, *7*, 117.
[44] W. Dong, M. Krbal, J. Kalikka, X. Y. Chin, B. Gholipour, C. Soci, P. Fons, K. V. Mitrofanov, L. Chen, R. E. Simpson, *Thin Solid Films* **2016**, *616*, 80.
[45] C. J. Diliegros-Godines, J. Santos Cruz, N. R. Mathews, M. Pal, *J. Mater. Sci.* **2018**, *53*, 11562.
[46] MATLAB documentation - globalsearch, https://www.mathworks.com/help/gads/globalsearch.html, (accessed: November 2022).